Preprint typeset using LaTeX style emulateapj v. 2/19/04

ON THE STRUCTURE AND EVOLUTION OF COMPLEXITY IN SIGMOIDS: A FLUX EMERGENCE MODEL

Archontis V.[1], Hood A.W.[1], Savcheva A.[2], Golub L.[2] and Deluca E.[2]

ABSTRACT

Sigmoids are structures with a forward or inverse S-shape, generally observed in the solar corona in soft X-ray emission. It is believed that the appearance of a sigmoid in an active region is an important factor in eruptive activity. The association of sigmoids with dynamic phenomena such as flares and coronal mass ejections (CMEs) make the study of sigmoids important. Recent observations of a coronal sigmoid, obtained with the X-Ray Telescope (XRT) on board Hinode, showed the formation and eruption phase with high spatial resolution. These observations revealed that the topological structure of the sigmoid is complex : it consists of many, differently oriented, loops that all together form two opposite *J-like* bundles or an overal S-shaped structure. A series of theoretical and numerical models have been proposed, over the past years, to explain the nature of sigmoids but there is no explanation on how the afore-mentioned complexity in sigmods is build up.

In this paper we present a flux emergence model that leads to the formation of a sigmoid, whose structure and evolution of complexity are in good qualitative agreement with the recent observations. For the initial state of the experiment a twisted flux tube is placed below the photosphere. A density deficit along the axis of the tube make the system buoyant in the middle and it adopts an Ω-shape as it rises towards the outer atmosphere. During the evolution of the system, expanding fieldlines that touch the photosphere at bald-patches (BPs) form two seperatrix surfaces where dissipation is enhanced and current sheets are formed. Originally, each of the bald-patch seperatrix surfaces has a *J-like* shape. Each one of the Js consist of reconnected fieldlines with different shapes and different relative orientation. The further dynamical evolution of the emerging flux tube results in the occurence of many sites that resemble rotational discontinuities. Thus, additional current layers are formed inside the rising magnetized volume increasing the complexity of the system. The reconnected fieldlines along these layers form an overall S-shaped structure. The reconnection process continues to occur leading to formation of another current concentration in the middle of the sigmoid where a flaring episode occurs. This central brightening is accompanied by the eruption of a flux rope from the central area of the sigmoid and the appearance of 'post-flare' loops underneath the current structure.

Subject headings: Solar Corona, Flux Emergence, Magnetic Reconnection

1. INTRODUCTION

X-ray observations of the solar corona (as recorded by several solar missions i.e, Skylab, Yohkoh, Hinode) have revealed the existence of structures with a forward or reverse S-shape. The forward S-shape structures are mainly formed in dominantly positive chirality regions (observed in the southern hemisphere) and more inverse S-shape structures have been observed to occur in negative chirality regions (northern hemisphere) (Pevtsov et al. 1997). The brightenings associated with these structures were named sigmoids by Rust & Kumar (1996), who also showed that many of the sigmoidal brightenings evolve into arcades, which are often associated with CMEs.

In general, the occurence of sigmoids in active regions is closely related to intense solar activity. Observational studies (Canfield et al. 1999; Canfield et al. 2007) have revealed that active regions with sigmoidal morphology are more likely to lead to eruptive events (flares or CMEs) than regions that do not possess sigmoids. Also, multi-wavelength observations (Pevtsov 2002) have indicated that there is a close spatial association between a coronal active region with an S-shape and chromospheric filaments. This connection may imply that sigmoids and filaments belong to the same topological structure. However, there is no evidence that all the filaments erupt during the brightening of the associated sigmoids.

Some sigmoids become bright only for a short period of time, usually just before the eruption. These sigmoids are called transient sigmoids and they tend to adopt one, single S-shape loop. In fact, observations have shown that many sigmoids have the shape of two *Js* or *elbows*, which together form the forward or reverse S-shape of the structure. In some cases, the twist within each of the two *Js* is such that the total twist in the sigmoid exceeds the threshold for the kink instability (Pevtsov et al. 1996). After the eruption, these sigmoids may evolve into post-flare cusped loops. Persistent or long-lived sigmoids, display the S-shape for considerably longer time than the transient sigmoids (for many hours, days or even weeks). It is likely that the shape of the persistent sigmoids is the result of many discrete sheared loops that keep their appearance for a long time period and all together form a sigmoidal structure. In this case, sigmoids possess a more intricate geometry. Observational examples of the different types of sigmoids and reviews on the evolution of sigmoids can be found in Canfield et al. (1999), Moore et al. (2001), Pevtsov (2002), Gibson et al. (2006a) and Green et al. (2007).

Recently a persistent coronal sigmoid with a complex morphology, observed with the XRT on board Hinode

[1] School of Mathematics and Statistics, University of St Andrews, North Haugh, St Andrews, Fife KY16 9SS, UK
[2] Harvard-Smithsonian Center for Astrophysics, 60 Garden st, Cambridge, MA02139, USA

(Golub et al. 2007; Deluca 2007). The high angular resolution of XRT provided a detailed view of the formation and evolution of this sigmoid. McKenzie & Canfield (2008) found that the sigmoid was not defined by a single X-Ray loop but it was consisted of many loops that they appear to define two *J-like* bundles. They also reported on the rising motion of a flux-rope-like structure from the middle of the sigmoid and the X-Ray flaring between the two J-shaped systems after the eruption of the flux rope. In our paper, we will present results from numerical experiments that might account for the occurence of such sigmoidal structures.

In the past years, a number of numerical experiments have been performed to describe the formation of S-shaped structures. A first batch of models (Moore & LaBonte 1980; Moore & Roumeliotis 1992) dealt with a sheared magnetic arcade. In these models the inner fieldlines at the core of the arcade are aligned along the polarity inversion line (PIL) and become curved to opposite sides at the ends of the PIL. Thus, the overal structure adopts an S-shape. The models suggest that tether-cutting reconnection occurs between the sheared fieldlines and as a result a flux rope is formed and eventually erupts. The resultant sigmoid is a transient sigmoid that occurs due to locally enhanced heating of the fieldlines becausee of their self-amplifying magnetic reconnection.

Kusano (2005) proposed the reversed-shear flare model for the self consistent formation of sigmoids and eruption, which is driven by magnetic reconnection above sigmoids. The simulation results suggested that if reverse shearing motion occurs in the inner part of a sheared arcade then the resistive tearing mode instability grows in the shearing inversion layer on top of the inner arcade. Magnetic reconnection is driven by the instabilty and eventually leads to formation of sigmoids and eruptive events. The process of reconnection occurs in a similar manner to the tether-cutting model.

It has also been suggested (Rust & Kumar 1996) that the sigmoid is part of a kinked flux rope. Indeed, numerical models (Török et al. 2004; Fan & Gibson 2003) have shown that the axis of the rope forms a forward or reverse S-shape structure. Another class of simulations studied the effect of photospheric twisting motions on a line-tied flux rope (Török & Kliem 2003; Aulanier et al. 2005; Gerrard et al. 2004). They showed that the current density becomes enhanced in a current layer, with a projected S-shape, below the flux rope or in a sigmoidal flux system at the lower part of the flux rope. These structures with enhanced current density might give rise to sigmoids.

An alternative model for the formation of transient sigmoids is the model by Titov & Demoulin (1999). They suggested that a current layer may develop along a quasi-seperatrix surface formed by bald-patch (BP) fieldlines that touch a rigid boundary, the photosphere. The BP fieldlines belong to a flux rope, which is (initially) force free. The dynamic evolution of the rope causes the dissipation in the sigmoidal bald-patch seperatrix surface (BPSS) to rise so that a transient sigmoid forms. In this model, there are two seperatrix surfaces associated with bald-patches (BPs) with a J-shaped morphology when they are projected onto a horizontal plane.

Experiments of flux emergence, from sub-photospheric layers up into the corona, have shown that emerging twisted flux tubes contain forward S-shaped but also reverse S-shaped fieldlines (Magara & Longcope 2001; Fan 2001; Fan & Gibson 2003, Archontis et al. 2004). For a right-handed twisted flux tube, the upper part of the windings of the fieldlines show an inverse-S shape while the lower parts are forward S-shaped, the latter being consistent with the observations. Thus, one might expect that sigmoids should be showing the concave upward segments of the twisted fieldlines of a flux rope. In a similar flux emergence experiment, Manchester et al. (2004) reported on the formation of a single sigmoidal current structure, along the PIL, at the dips of sheared and stretched fieldlines. A flux rope is formed above the current sheet due to reconnection of fieldlines along the current structure. Eventually, the flux rope rises into the corona.

All the above simulations have provided important physical insight towards the understanding of the process of formation of sigmoidal structures. However, none of the above simulations have shown how sigmoids, which are persistent and complex in geometry, are formed in a self-consistent way. As we mentioned above, recent observations show that sigmoids consist of multiple loops and that are not a continuous S-shape structure. They also show the occurence of two J's, which are brighter than the central part of the sigmoid most of the time, while during the eruption the central part develops a very bright bar-shaped region. The latter might account for an erupting flux rope. The results presented in this paper are in good qualitative agreement with these observations.

The layout of the present paper is as follows: Section 2 presents the equations and the model used in the numerical experiments. Section 3 describes the initial phase of the rising motion of the emerging field. The topology of the fiedlines of the emerging field is discussed in Section 4. The complex geometrical shape and the evolution of the current structures, which are formed inside the magnetized rising volume are presented in Section 5 and 6 respectively. Section 7 presents the evolution of the temperature and density distribution along the sigmoid. Qualitative comparison of the numerical results with new observations, as recorded by the X-Ray Telescope on board Hinode, are presented in Section 8. Section 9, finally contains a summary of conclusions and discussion.

2. MODEL

The numerical setup for this experiment is similar to the work of Archontis et al. (2004). The code used to simulate the evolution of the model is a 3D version of the Lagrangian remap scheme detailed in Arber et al. (2001). We used the above code to perform experiments with uniform resistivity and with locally enhanced resistivity , so that the resistivity is switched on only when the current has exceeded some critical value. The general evolution of the system is similar in the two sets of experiments. Hereafter, we show the evolution in the experiments where resistivity is uniform, with a value of $\eta = 10^{-3}$. The code also includes small shock viscosity and viscous heating.

For the experimemts described in the paper, we solve the time-dependent, resistive, MHD equations in three dimensions. They are written in the form

$$\frac{\partial \rho}{\partial t} + \nabla \cdot (\rho \mathbf{u}) = 0, \quad (1)$$

$$\frac{\partial (\rho \mathbf{u})}{\partial t} = -\nabla \cdot (\rho \mathbf{u}\mathbf{u}) + (\nabla \times \mathbf{B}) \times \mathbf{B} - \nabla P + \rho \mathbf{g}, \quad (2)$$

$$\frac{\partial (\rho \epsilon)}{\partial t} = -\nabla \cdot (\rho \epsilon \mathbf{u}) - P \nabla \cdot \mathbf{u} + Q_{\rm Joule} + Q_{\rm visc}, \quad (3)$$

$$\frac{\partial \mathbf{B}}{\partial t} = \nabla \times \left(\mathbf{u} \times \mathbf{B} \right) + \eta \nabla^2 \mathbf{B}, \quad (4)$$

with specific energy density

$$\epsilon = \frac{P}{(\gamma - 1)\rho}. \quad (5)$$

The basic quantities used in the above equations are the density ρ, the pressure P, the magnetic field vector $\mathbf{B}$ and the velocity vector $\mathbf{u}$. $Q_{\rm Joule}$ is the Joule heating term due to resistive losses and $Q_{\rm visc}$ is the viscous dissipation, $\mathbf{g}$ is the gravity and is taken to be uniform in the z-direction, η is the resistivity and γ is the ratio of specific heats.

The equations are solved in a uniform grid of (256,256,320) in the (x,y,z) directions and the physical size of the box is 34 Mm x 34 Mm x 27.2 Mm. We use a uniformly spaced coordinate system in the horizontal directions x and y, with increased resolution in z from -4.25 Mm to 22.95 Mm. The background stratification includes a constant-entropy region of 6 Mm thickness that simulates the uppermost layers of the solar interior just below the surface; an isothermal layer ($T = 6500$ K) with thickness 1.7 Mm that represents the *photosphere* and the *chromosphere* and an isothermal *corona* at $T = 10^6$ K with thickness 19.5 Mm. The photosphere and chromosphere are joined to the corona through a transition region with a steep temperature gradient.

Figure 1 shows the gas pressure, temperature, magnetic pressure and density of the stratified environment as a function of height. All the profiles are normalized according to the photospheric values: $p_{ph} = 1.4\,10^5$ erg cm^{-3}; $\rho_{ph} = 3\,10^{-7}$ g cm^{-3}; $T_{ph} = 5.6\,10^3$ K and $H_{ph} = 170$ km. Other derived units used in the simulations are: velocity, $V \equiv (p_{ph}/\rho_{ph})^{1/2} = 6.8$ km sec^{-1}; time, $t_{ph} = V/H_{ph} = 25$ sec and magnetic field, $B_{ph} = \sqrt{p_{ph} 8\pi} = 1.3\,10^3$ Gauss.

A horizontal magnetic flux tube with axis at $y = 0$ and twisted field lines is situated below the photosphere. Initially, it is in pressure balance with its surroundings. Then, the tube is made buoyant through a density deficit which peaks towards $x = y = 0$. More precisely, the deficit is reduced as one goes from the center (where the tube temperature equals the external temperature) towards the ends of the tube following the gaussian profile:

$$\rho = \rho_b(z) + \rho_{def} e^{\frac{-y^2}{\lambda^2}}, \quad (6)$$

where $\rho_b(z)$ is the background density profile and ρ_{def} is the density deficit and is negative. The density deficit is specified as:

$$\rho_{def} = \frac{P_{def}}{\rho_o(z)} P_o(z), \quad (7)$$

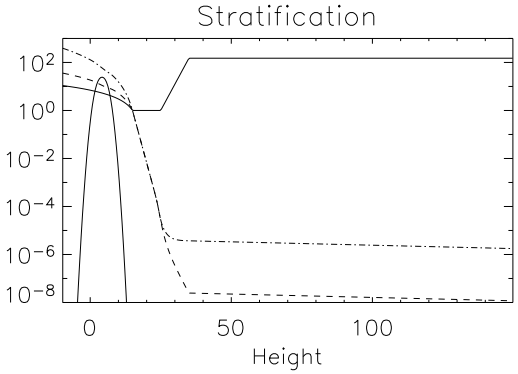

FIG. 1.— Distribution of temperature (solid line), pressure (dot-dashed), density (dashed) and magnetic pressure (thick solid line) along height ($x = 0, y = 0$) at $t = 0$.

where $P_o(z)$ and $\rho_o(z)$ are the pressure and density of the background atmosphere, respectively. We require the tube to be in radial force balance with the external plasma. Thus, we require:

$$P_{def} = -\frac{d(B^2/2)}{dr} - \frac{B_\theta^2}{r}, \quad (8)$$

where B_θ is the azimuthal component of the magnetic field, defined as:

$$B_\theta = \alpha r B_y, \quad (9)$$

In the above equations, α is the twist of the fieldlines about the tube's axis. The parameter λ represents the half length of the buoyant part of the tube and the density deficit has its maximum value at the center, generating the classical Parker buoyancy instability. Thus, the tube adopts the shape of an Ω loop as it rises.

The central section of the tube first rises towards the photosphere and then subsequently on into the corona. The initial value of the radius of the tube is $R = 2.5$ ($\approx 425km$). The axial magnetic field component, B_y, is given by a simple Gaussian profile

$$B_y = B_0 \exp\left(-\frac{r^2}{R^2}\right), \quad (10)$$

where $r = \sqrt{x^2 + (z - z_c)^2}$ is the radial distance from the axis of the tube, initially located at a height z_c. The magnetic field strength on the axis of the tube is $B_0 = 5$ ($\approx 6.5KG$). This field strength corresponds to a local plasma $\beta = 5.4$ at the axis of the tube, with β being the ratio of the gas pressure to the magnetic pressure.

The magnetic field lines are uniformly twisted around the central axis of the tube, $B_\varphi = \alpha r B_z$, with B_φ the azimuthal component of the magnetic field in the xy plane and $\alpha = 0.4$. With this twist, the tube is marginally stable to the kink instability. The twist is right-handed and so is appropriate for emergence in the southern hemisphere.

3. RISE OF THE FIELD INTO THE CORONA

The initial phase of the emergence of the tube is very similar to that described in Archontis et al. (2004), where a flux tube rises into a non-magnetized corona. A recent review on models of magnetic flux emergence can

be found in Archontis (2008). In the following, we review some of the essential features of the initial rising phase and expansion into the higher levels of the stratified atmosphere.

The buoyant flux tube rises through the lower level of the atmosphere and at $t = 28$ the upper part of the rising magnetic sytem reaches the photosphere. During the rise the plasma in the tube expands due to a density contrast of about 10 between the initial height of the tube and the base of the photospheric layer. The size of the tube also increases, but the increase is less than a factor of 2. The rising motion of the crest of the tube is slowed upon reaching the photosphere, due to the change in the background stratification, from the adiabatically stratified interior to the isothermal and strongly sub-adiabatic photosphere. When the tube reaches the photosphere a bipolar region is formed. The fieldlines that join the positive with the negative polarity have a north-south orientation due to the initial strong twist of the fieldlines. Eventually, the bipolar region moves towards an east-west direction (Figure 2, left panel where the colored plane shows contours of the photospheric vertical magnetic field component) as more internal magnetic layers rise to the photosphere and the inclination of the anchored legs of the tube beneath the photosphere becomes more vertical.

As the two polarities are moving in opposite directions along the neutral line, shearing of the field occurs so that the magnetic field lines lose their strongly azimuthal nature and run nearly in parallel to the neutral line. The middle panel in Figure 2 shows the longitudinal component of the velocity field, v_y, at photospheric heights. The shear flow can reach up to 10 km/sec. The shear flow is relatively enhanced close to the two main polarities of the system.

The fieldlines shown in Figure 2 reveal the effect of the shearing and the lateral expansion on the topology of the magnetic field. The *inner* fieldlines, which have been traced from points closer to the polarity inversion line, are lying mostly along the neutral line due to the intense shearing. The fieldlines further from the neutral line are more perpendicular to the initial axis of the tube and outline the outer edge of the expansion of the system.

Eventually, the dense plasma on the magnetic field is transported into the corona via the magnetic buoyancy instability experienced by the plasma above the photosphere. The criterion for this local instability has been given by Acheson (1979) and used by Archontis et al. (2004) to describe the emergence of flux into the outer atmosphere in simulations similar to the present numerical experiments. The advance of the flux tube into the upper atmosphere is accompanied by another marked expansion of the rising field due to the decrease of the background gas pressure with height.

An important factor for the emergence of the tube through the photosphere and into the outer atmosphere is the plasma β.

$$\beta = \frac{P_g}{P_m}, \tag{11}$$

where P_g and P_m are the gas and magnetic pressures. In general, the magnetic pressure is larger than the gas pressure inside the expanding volume of the rising tube and the corresponding force drives the dynamical evolution of the system. It is worthwhile mentioning, however, that the plasma β does not have a uniform distribution along the neutral line at low photospheric heights. This is shown in the right panel of Figure 2, where plasma beta is visualized at a horizontal slice, $z = 15$, at the base of the photosphere. The distribution of β with values less than one shows an S-like shape, which has its middle part stretched along the neutral line of the bipolar region and the two ends curved around the positive and negative polarities. It has lower values at the vicinity of the two polarities where the emerging field is stronger (by a factor of 2) compared to the middle part of the emerging field. This is because the central area of the emerging field intersects the photosphere earlier than the other upcoming layers. It spreads out horizontally in a short time scale and its magnetic field becomes relatively weak. The right panel in Fig. 2 shows that plasma beta at the central part of the emerging field is $\beta \approx 0.5$, a factor of 5 larger than at the ends. Therefore, the emergence of the field to the outer atmosphere becomes dynamically more efficient as one moves from the center towards the ends of the neutral line of the bipolar region.

In previous simulations (Manchester et al. 2004; Gibson & Fan 2006; Archontis & Hood 2008), it has been shown that as the magnetic field rises above the photopshere and expands, the sheared magnetic fieldlines are also stretched vertically. Thus, sheared fieldlines with opposite directions come closer together and, as a result, the current density ($\mathbf{J} = |\nabla \times \mathbf{B}|$) becomes large in the region between them. The current structure, and the fieldlines that surround the current, have an S-like shape adopting the twist and writhe of the underlying field.

In this section, we showed that the distribution of plasma β is reminiscent of a sigmoidal structure, oriented along the main axis of the buoyant tube. Also, the values of plasma β are smaller along the two curved parts of the sigmoidal structure and, thus, we expect that the actual emergence and the subsequent vertical stretching of the fieldlines to be more effective at these sites. Moreover, the current density should be larger (accompanying the stretching and shearing of the field) at the afore-mentioned regions, forming two oppositely curved *elbows* or *J-like* structures. Indeed, the formation of two *elbows* with enhanced current density inside an emerging flux region has been recently shown in the model by Archontis & Hood (2008). That model investigated the interaction between two rising flux tubes. The two *elbows* were formed on opposite sides of the neutral line of the first emerging flux tube. The straight part of the *elbows*, close to middle of the sigmoidal structure, sheared past each other and were ready to reconnect when they came into contact.

The present model investigates the formation and evolution of current structures inside a *single* flux system. In the next sections, we will show that, during the early evolution of the system, the current density is smaller at the middle of the neutral line and larger at the *elbows*. However, as time goes on the current is enhanced at the central region and the distribution of the current density inside the three-dimensional expanding volume becomes increasingly complex.

Before we illustrate the three-dimensional structure of the current and its temporal evolution, it is important to study the shape of individual fieldlines associated with

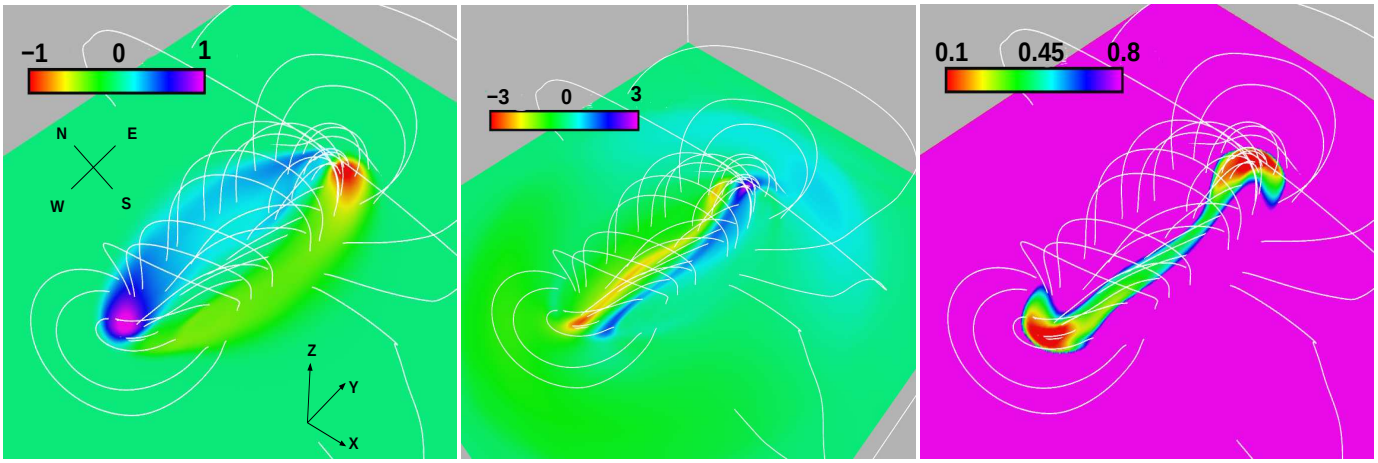

FIG. 2.— *Left:* 2D visualization of B_z together with fieldlines at $t = 110$. *Middle:* The same as in the left panel but for the longitudinal component of the velocity field, v_y. *Right:* The same as the other panels but for the plasma β. A color version of this figure is available in the electronic edition of the Astrophysical Journal.

the current structures and follow their topology in time. This will help us to understand the linkage between the *elbows* and the geometry of the magnetic field. We elaborate on this in the next section.

4. TOPOLOGY OF FIELDLINES AND BALD PATCHES

In this section, we show sets of fieldlines, traced from the same locations, at three different times during the early evolution of the system. More precisely, Figure 3 illustrates the three-dimensional expansion of three sets of fieldlines (lines in white, red and yellow color) at $t = 100$, $t = 110$ and $t = 120$. The horizontal slice shows the vertical component of the magnetic field, B_z at $z = 15$. Two views are shown: front (left panels) and top (right panels). We choose to trace the fieldines from three selected regions along the inversion line of the bipolar region. The fieldlines have a concave upward shape at the sites where they touch but do not cross the base of the photosphere. These sites are called bald-patches.

The magnetic fieldlines touching a BP, form dips which become favourable sites for capturing dense material from the low atmosphere. It is known that dense plasma may well be supported by magnetic tension in these dips, as illustrated by Priest et al. (1989) for filament support. The lifting of the dense material into the corona, when the higher parts of the fieldlines move upward, is observed during, for example, the rise of a prominence. Also, shearing motions of photospheric magnetic field elements and the upward movement of fieldlines that touch BPs may naturally lead to formation of strong current structures (Gibson & Fan 2006). The latter may imply the action of magnetic reconnection and the manifestation of intense heating. In general, BPs are thought to play an important role in flares and filament formation (Titov et al. 1993).

The white lines are fieldlines that possess a BP at the central part of the inversion line. They reach large coronal heights close to the two main polarities of the emerging field, before going all the way down to the subphotospheric layer where they are anchored. Notice that they have a full rotation *above* the photosphere, adopting a smooth sigmoidal shape when they are projected onto a xy-horizontal plane (top view). The other sets of fieldlines are tangent to the photosphere at two segments,$102 < y < 105$ and $48 < y < 51$. The red fieldlines have been traced from the region close to the positive polarity (W) and the yellow fieldlines from the area close to the negative polarity (E) of the magnetic field. At the beginning of the evolution (t=100) the two sets of fieldlines pass through both photospheric segments (called BP1 and BP2 in panel A) and they expand at three different locations: at the center where they envelop the crest of the emerging field and in the close proximity of the two polarities, where they expand sideways. Due to the initial strong twist, these fieldlines undergo more than one full turn along the buoyant part of the tube at the photosphere.

It is interesting now to follow the evolution of the sets of fieldlines that pass through the same photospheric segments. During the evolution, the concave part of the white fieldlines covers a substantial horizontal distance, since they connect the two sides of the middle part of the oval-like shaped, emerging flux region. Note that the concave parts of the fieldlines are favourable sites for the accumulation of dense and cool plasma, which in turn may obstruct the full emergence of the fieldlines and the axis of the tube into the corona. Indeed, the white fieldlines at this central BP retain their flat, straight and long horizontal shape at the same photospheric height between $t = 100$ and $t = 120$. On the other hand, the parts of the white fieldlines that connect directly the central BP region with the two polarities of the emerging field, are free to rise and expand into the higher levels of the atmosphere, as seen in Panels B and C. Following the windings of these white fieldlines in time, we see that they run along a larger distance (due to the dynamic expansion), from the central BP towards the two polarities, forming an elongated S-shape along their length.

The yellow and red fieldlines evolve in a different way than the white fieldlines. The red (yellow) fieldlines, which are traced from the region close to BP1 (BP2), are eventually detached from the photospheric bald batch BP2 (BP1). Indeed, at $t = 120$, the red (yellow) fieldlines establish direct loop-like connection with the negative (positive) polarity of the emerging field without passing

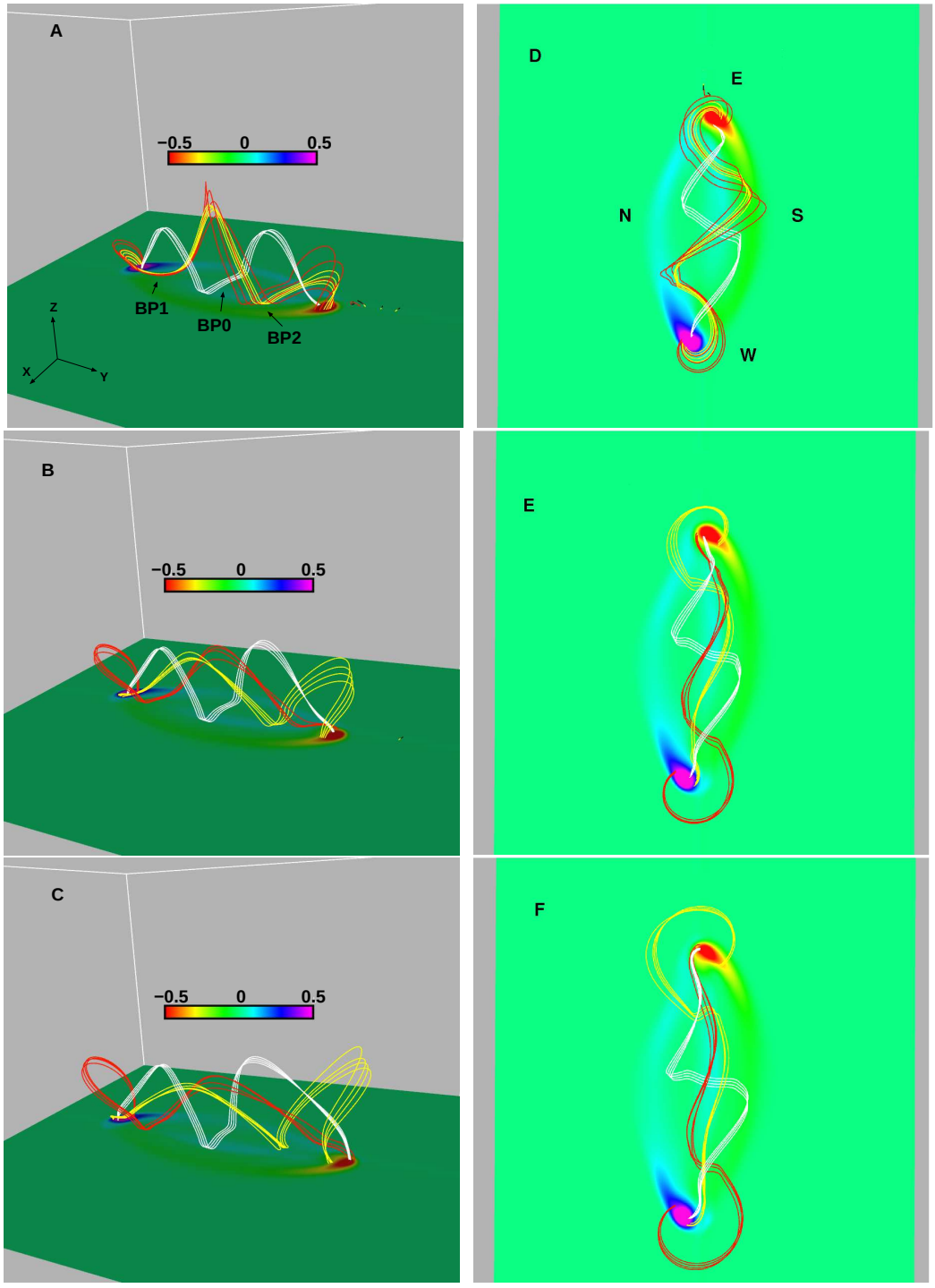

FIG. 3.— Two series of panels at $t = 100$, $t = 110$ and $t = 120$ illustrating the evolution of fieldlines that pass through the same photospheric segments at these snapshots. Panels A-C show three different sets of fieldlines. The white fieldlines have been traced from the central bald-patch BP0, the red fieldlines from the BP1 and the yellow fieldlines from the BP2. The horizontal contour shows the vertical component of the field, B_z, at the photosphere. The panels D-F are the corresponding top-view images for the same times. A color version of this figure is available in the electronic edition of the Astrophysical Journal.

first through the BP2 (BP1).

The change in the connectivity of these fieldlines is due to an internal reconnection that occurs when oppositely directed fieldlines come into contact due to vertical stretching and horizontal shearing of the field. As we mentioned in the previous section, the dynamical emergence of the twisted field and the subsequent vertical stretching and internal reconnection are more pronounced at the regions close to the two polarities. Thus, the connectivity of the fieldlines is expected to change more efficiently at these regions. Similar events due to internal reconnection at low heights have been described

in the models by Manchester et al. (2004), Gibson & Fan (2006) and Archontis & Hood (2008).

The magnetic topology, formed by the red and yellow fieldlines considered in Figure 3, is similar to the topological structure produced in the model by Titov & Demoulin (1999). The initial configuration in their model consists of a force-free flux tube with an arch-like shape that rises quasi-statically into an external potential magnetic field. Eventually, the tube becomes unstable, leading to an eruption of magnetic flux. Titov & Demoulin (1999) described how separatrix surfaces are formed by fieldlines, which start at a BP. These surfaces are called bald patch separatrix surfaces (BPSS) and the fieldline connectivity has a jump across it. When these surfaces are projected onto a horizontal plane, two *J-like* structures are identified, each one of them associated with BPs.

In our model the fieldlines that form the bald patch separatrix surfaces are the red and the yellow lines. The top view at $t = 120$ (panel F, Figure 3) shows that the red (yellow) fieldlines reveal a structure with a *J-like* shape, with the curved part of the J to be at the west (east) side of the emerging magnetic field. The two separate sets of fieldlines are wrapping around each other along the neutral line, but their overal projection onto the photospheric plane forms a sigmoidal structure.

Now, these fieldlines are rooted in the photosphere at BP1 and BP2 by the dense plasma and, when their coronal parts move upwards, they become highly stretched. In fact, the evolution in Figure 3 shows that the red and yellow fieldlines touch the photosphere (at BP1 and BP2 correspondingly) along a shorter horizontal distance in time, due to this stretching. This leads to the appearance of a locally strong current concentration.

The top panel in Figure 4 shows the time evolution of the maximum value of current density at BP0 (dashed curve), BP1(solid) and BP2 (dot-dashed). The bottom panel shows the average horizontal distance along which the fieldlines touch the photosphere at the central region of each BP. The temporal evolution of current shows a pronounced increase up to time $t = 110$, followed by an imperceptible enhancment until t=120. The horizontal distance keeps a good anti-correlation with the change in the current density. During the first phase, the horizontal distance decreases substantially because of the stretching of the field and thus the current, which is build up at the BPs, increases. As time evolves ($t = 110$), the current increases towards its maximum value and internal reconnection starts to occur between oppositely directed vertical fieldlines on either side of each of the BPs. After the first instance of internal reconnection, the horizontal distance undergoes a more moderate decrease, possibly due to less effective stretching of the new fieldlines that intersect the photosphere at BP1 and BP2.

5. STRUCTURE OF THE CURRENT

Figure 5 shows the distribution of the current density at low photospheric heights, together with fieldlines to understand the linkage between the current concentration and the topology of the magnetic field. The isosurface (in light green color) shows that the current is pronounced at the curved parts of the *elbows* and at the dips of the fieldlines, at the close neighborhood of BP1 and BP2. The value of **J** corresponds to 95% of the

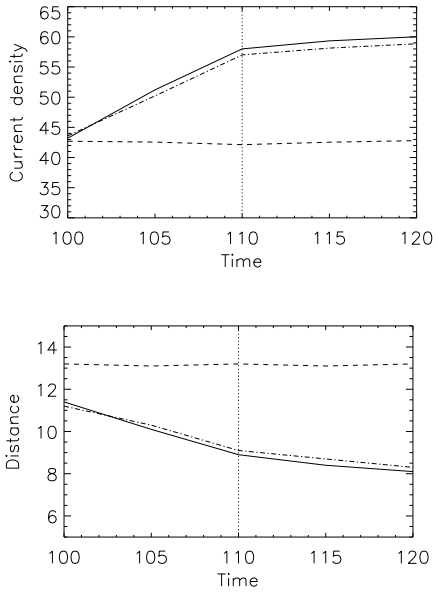

FIG. 4.— *Top:* Time evolution of the maximum value of **J** at the bald patches. BP0 is shown by the dashed line, BP1 with the solid and BP2 with the dot-dashed. *Bottom:* Time evolution of the average horizontal length scale of the same BPs at the photosphere.

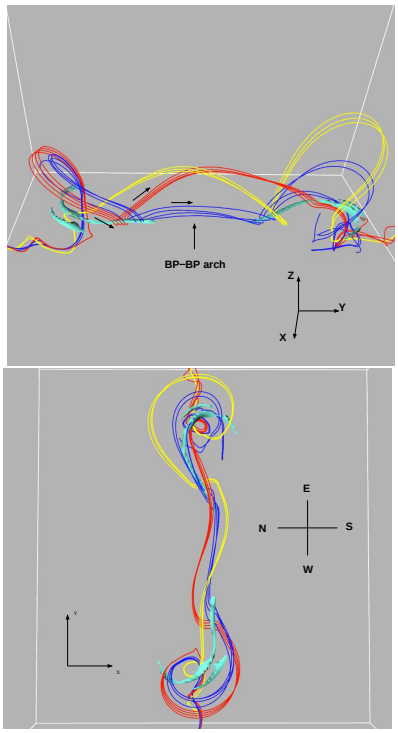

FIG. 5.— *Top:* Three-dimensional representation of fieldlines at time $t = 120$. The green isosurface represents high values of current density at the base of the photosphere. *Bottom:* Top view of the same visualization. The horizontal projection of the fieldlines and the current concentration shows a structure with an *S-like* shape. A color version of this figure is available in the electronic edition of the Astrophysical Journal.

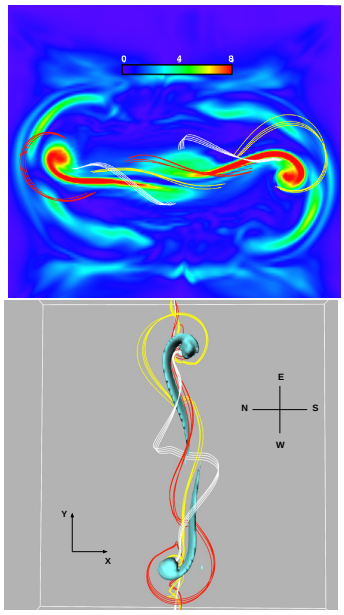

FIG. 6.— *Top:* A two-dimensional color represenation of the current density at $z = 28$ and $t = 120$. Maximum values of the current density are found along the two *J-like* structures. The fieldlines overplotted in this figure are the same with the fieldlines in Figure 3. *Bottom:* Top view of the 3D representation of the fieldlines. The isosurface shows the regions above $z = 28$ where the current density has large values. A color version of this figure is available in the electronic edition of the Astrophysical Journal.

maximum current density at this snapshot. Moreover, the projection of the current distribution in a horizontal plane (bottom panel) shows that it is distributed along the two *J-like* structures, as we expected from our previous considerations. The red and yellow fieldlines are the same fieldlines with those in panel F of Figure 3. The blue fieldlines are the only fieldlines grazing the photosphere twice, at points belonging to the close vicinity of BP1 and BP2. These fieldlines are similar to the special line, called 'BP-BP line' or 'separator' in the Titov & Demoulin (1999) model. They consist of three loops: the central loop that connects BP1 with BP2 determines the arch along which the BPSS intersect, while the two peripheral loops may act as contact layers or *borders* between the two separatrices.

Figure 6 shows the distribution of current density at higher levels of the atmosphere. This is shown by the top panel, which shows the projection of the current density onto a two-dimensional xy-plane. The value of the current density isosurface is less compared to the corresponding value at lower heights. However, it is evident that the current remains strong along the two *Js*.

In a similar manner, the bottom panel of Figure 6 shows the 3D isosurface of the current with the highest magnitude at heights above $z = 28$. The value of the isosurface is a factor of six less than the current isosurface visualized in Figure 5. Thus, the current density retain the shape of the two *Js* at different levels of the atmosphere, but the magnitude inside these structures decreases with height. Also, the fieldlines on the opposite (north and south) sides along the *J-like* structures are different, when one looks at different heights.

At low heights, the oppositely directed field on the two sides of the *Js* belongs to the same fieldlines (for example, to the blue fieldlines that pass below the current in Figure 5). The internal reconnection, mentioned in the previous sections, is the reconnection of these fieldlines and occurs along the low-lying *Js*. Due to reconnection, two flux tubes are formed, one above each of the current concentrations (see panels A and B in Figure 7). Eventually, the flux tubes rise to the outer atmosphere.

At large heights, the *elbows* are located between different sets of fieldlines. For example, the west-side *elbow* is formed between the red, the yellow and the white fieldlines. White and yellow fieldlines are coming from below the photosphere and intersect with it at the north part of the field pointing upwards, while the red fieldlines run towards the photosphere pointing downwards. The fieldlines at these heights do not suffer from vertical stretching but they rather expand into the atmosphere. Thus, the local horizontal distance across the *elbows* is larger than at lower heights and the current density is smaller. This current, with a *J-like* shape at large heights, is the *bulk* current of the flux tubes and is carried within them as the tubes rise. The red, yellow and white lines are the magnetic fieldlines that surround the flux tubes in a small distance from the central region of the tubes.

Figure 7 shows the internal reconnection of fieldlines at low heights and the strong current concentration below the rising flux tube. Panel A shows the total current density with a value of $|\mathbf{J}| = 3$ for $z > 25$ (isosurface in yellow color). The vertical slice shows the full magnetic field vector at $y = -26$. The cross section of the flux rope is shown just above the isosurface of current. Panel B is a two-dimensional vertical cut at $y = -26$ and shows the distibution of the longitudinal component of the current, J_y. The current is strong at the vertical current sheet where fieldlines reconnect. It is also non negligible inside the rising flux tube where it has moderate values. Panels C and D show a three-dimensional representation of the topology of the fieldlines around the low-lying *J-like* structure of current (transparent isosurface) and the rising tube. The blue fieldlines go below the current concentration and have dips at the close neighborhood of BP1. The orange fieldlines are reconnected fieldlines and have been traced from inside the current structure and below the flux tube. The green fieldlines go through the central area of the flux tube at $y = -26$, near the tip of the arrow in panel A. Panel D shows that these fieldlines come from the positive polarity region of the emerging field and run above the full length of the *J-like* structure before they dive down, below the axis of the original flux tube, at the photosphere. Similar (to the green) fieldlines are found in the north side of the emerging region and belong to the flux tube, which rises above the other *J-like* structure.

The first events of internal reconnection happen at heights below the transition region, where density is large. The dips of the fieldlines that reconnect are filled up with this dense plasma. Thus, when the flux tubes are formed and rise above the *Js*, dense material is lifted to the outer atmosphere.

6. EVOLUTION OF THE CURRENT

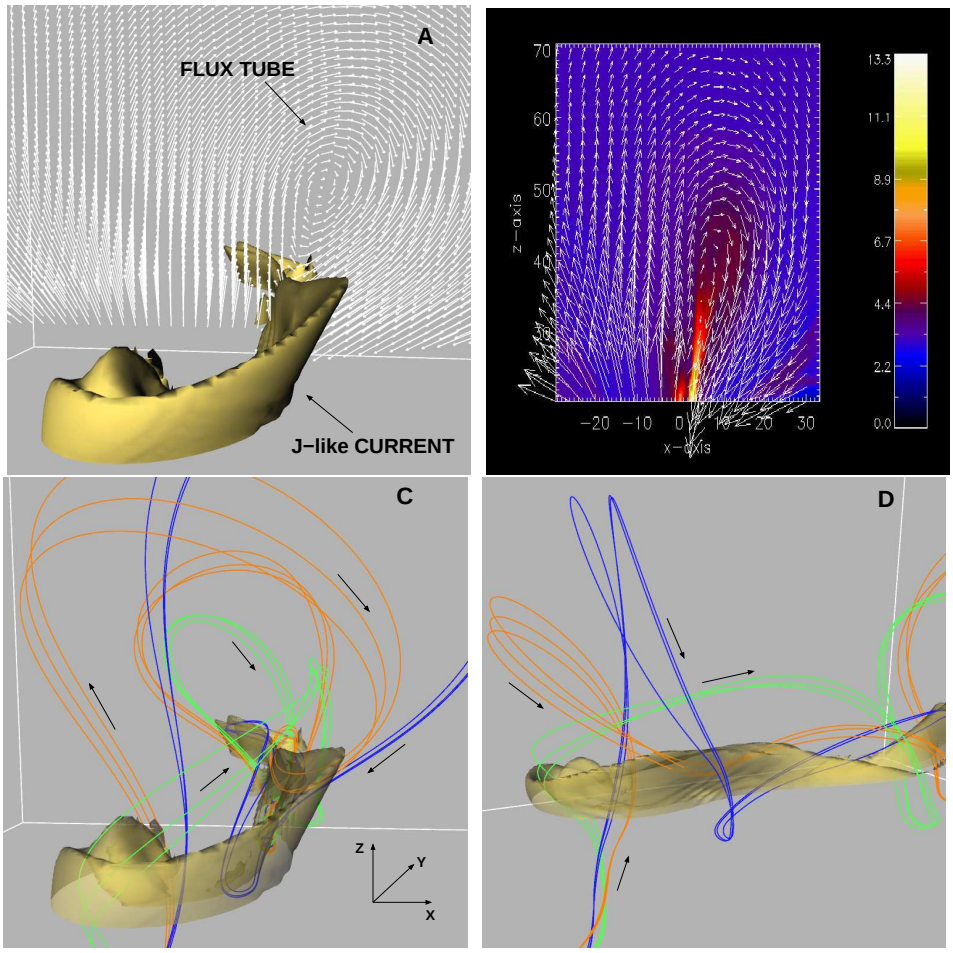

FIG. 7.— Panels A and B show the formation of a flux tube above a strong current concentration. The current density is visualized with the transparent isosurface. Superimposed is the magnetic field vector (arrows). The colormap in panel B shows Jy. Panels C and D show a visualization of the field line topology around the current structure. Shown are selected fieldlines involved in the reconnection process at three different heights: below the current (blue lines), inside the current (orange lines) and within the rising flux tube (green lines). The arrows in panels C and D show the sense of the magnetic field vector. A color version of this figure is available in the electronic edition of the Astrophysical Journal.

It is now important to follow the evolution of the current density during the dynamical emergence of the field. To illustrate the geometry of the current, we visualize in Fig. 8 the three-dimensional structure of current density for three different times. The value of the current, which is visualized by the isosurface in this figure, is the same for all snapshots. For clarity reasons, only a sample of the whole computational box is shown (from the upper photosphere to the middle of the corona). The right column in Figure 8 shows different sets of selected fieldlines, which have been overplotted on the transparent isosurface of the current density.

Looking at the isosurface in panel A, one sees that at the beginning the current is confined along the two *J-like* structures. In panel D, red and yellow fieldlines have been traced from the north and south-side *Js* respectively. Notice, that *all* the fieldlines have dips below the isosurfaces and there are no fieldlines that connect directly the positive with the negative polarity of the emerging field yet. Also, the red fieldlines, which run along the current isosurface at the south side, envelope the other J from above. Thus, the red fieldlines might work as ambient fieldlines for the rising tube above the north-side *J-like* structure. The yellow fieldlines do the same on the other side of the emerging system.

At $t = 140$ (panel B), the electric current becomes more rich in structure, as additional current surfaces appear inside the sigmoidal volume. Such surfaces are shown by the arrows in this panel. In fact, these additional current surfaces are closely associated with the central region of the rising tubes above the two initial *elbows* (current-carrying flux tubes). More precisely, they go through the cross section, at each vertical slice, along the rising tubes at the south and north sides of the emerging region. This is illustrated through the inset in panel B: it shows a close-up of one of these isosurfaces and a vertical slice with the full magnetic field vector.

Panel E shows fieldlines (in red, yellow and white color), which are traced from the isosurfaces shown by arrows in panel B. These fieldlines come /it directly from the positive polarity region and they are twisted as they run in parallel to the isosurfaces. All the fieldlines in panel E pass through the lower photosphere and so possess dips at low heights. The blue fieldlines, have been

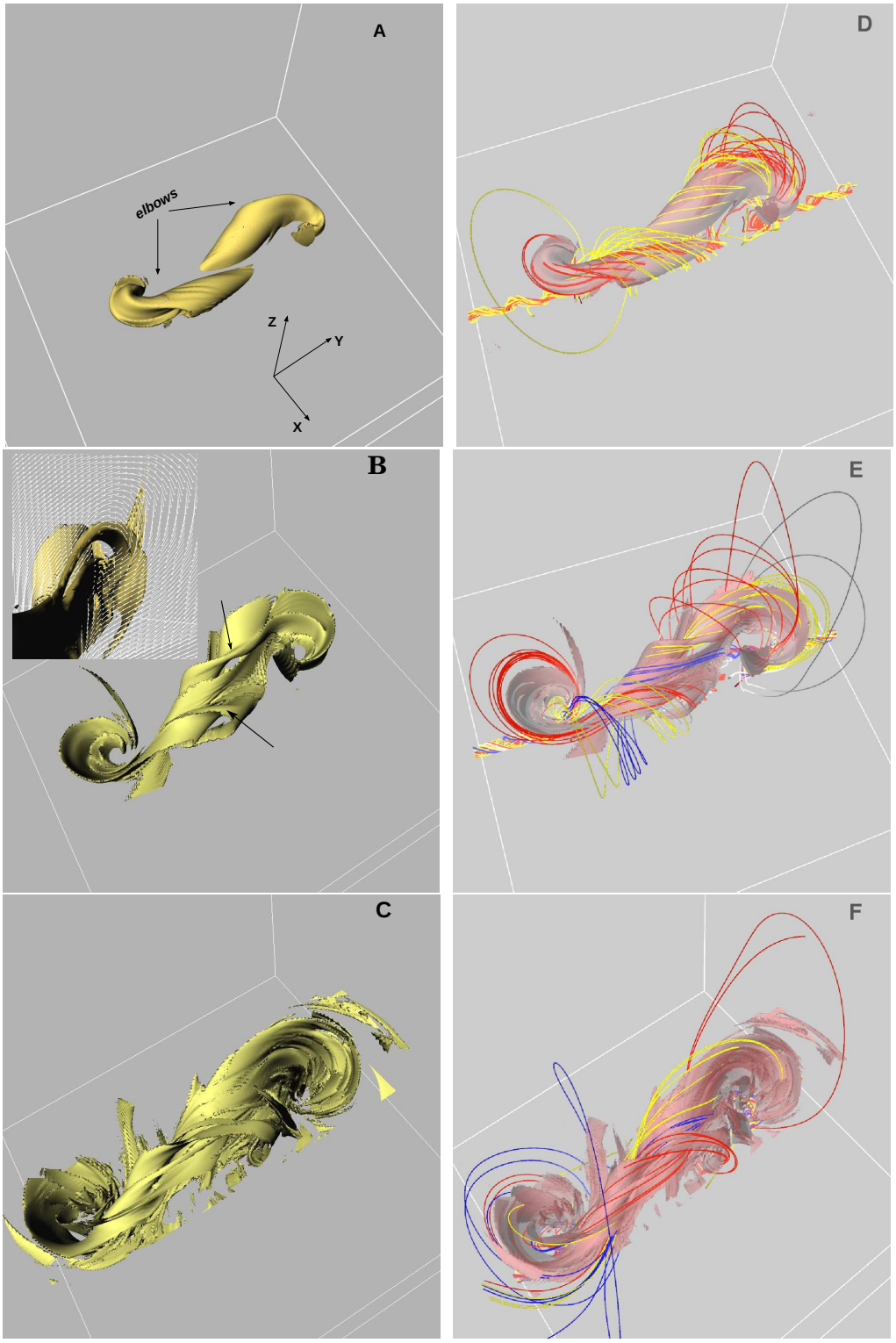

FIG. 8.— High current density isosurfaces illustrating the evolution of the sigmoidal structure. Times are $t = 120$, $t = 140$ and $t = 184$ for the upper, middle and lower row respectively. The fieldlines, which are shown in the right column, are selected fieldlines traced from various regions along the isosurfaces. The little inset in panel B shows that some of the isosurfaces accompany the rising flux tubes. The general evolution of the current density , shown in the panels A-F, document a case of a sigmoid that consists of many current layers. A color version of this figure is available in the electronic edition of the Astrophysical Journal.

traced from the area between the two *Js*. Similar to the other fieldlines, they complete more than one full turn from one polarity to the other. At this time of the evolution, there are no fieldlines that have fully escaped into

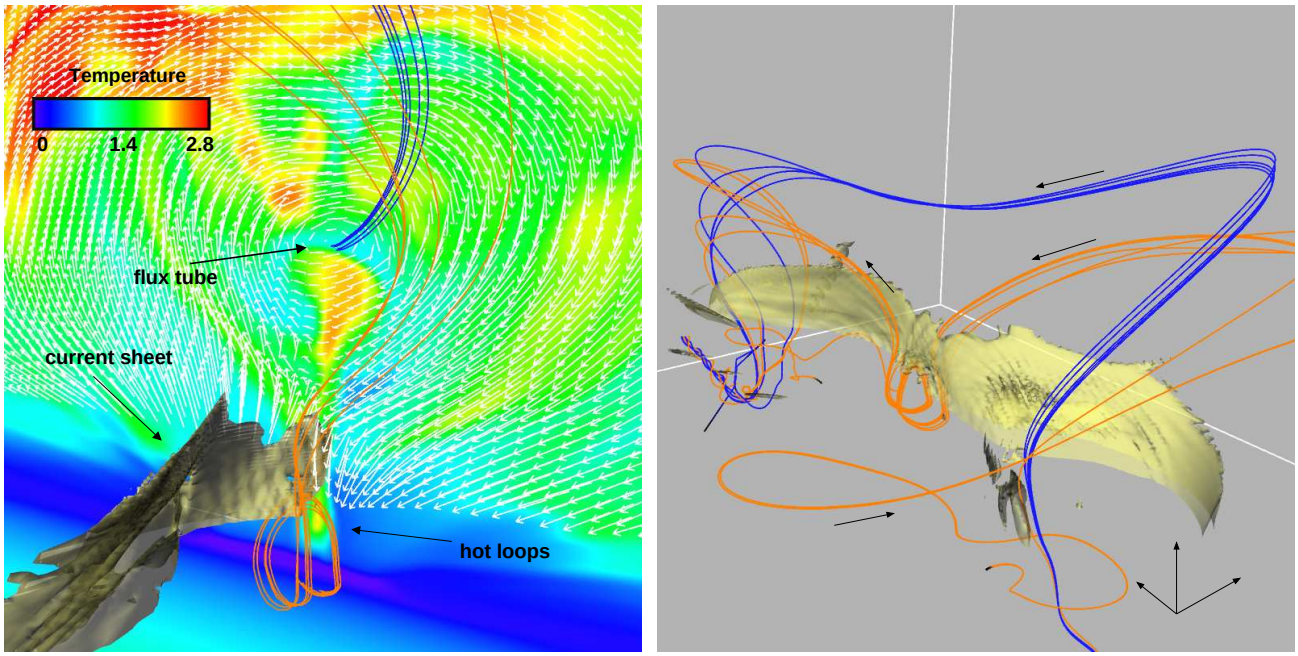

FIG. 9.— *Left:* Rise of a flux tube at $t = 180$. The temperature contours (in logarithmic scale) are on the plane $y = 0$. An isosurface of enhanced current density and the full magnetic field vector (arrows) are superimposed. *Right:* Full view of the three dimensional current sheet and the topology of the fieldlines. The arrows show the direction of the magnetic field. A color version of this figure is available in the electronic edition of the Astrophysical Journal.

the corona.

At later times ($t = 184$), the current adopts an even more pronounced filamentary structure (see panels C and F). The structure includes a multiplicity of twisted current filaments and layers, arranged in the form a sigmoidal shape. This complexity is apparent not only around the middle part of the sigmoidal structure but also at the ends. The latter resemble spiral scrolls, which in fact seem to be increasingly twisted during the sigmoid evolution.

The reason for the appearance of a considerable number of current layers is as follows. At low heights, new currents are formed when the fieldlines, that still have dips, come closer together. This process that leads to intense current concentration in between the fieldlines, is due to shearing and stretching of the emerging field as has been described in the previous section. At later times of the evolution, this also occurs around the central region of the neutral line. The yellow and blue fieldlines in panel F are the result of this process. They are reconnected fieldlines, which have been traced from newly formed, low-lying current structures at the central region of the sigmoidal structure. The majority of the reconnected fieldllines do not have dips along their lengths. Their projection onto horizontal planes adopt sigmoidal shapes, running from the one end of the overall sigmoidal structure to the other, which are rising and expand into the corona. Such fieldlines do not exist at earlier times during the emergence (see panels D and E). We should mention that a result of this late internal reconnection is the formation of a flux tube, which rises above the central region of the sigmoidal structure. The expulsion of the flux tube is accompanied by intensive heating (see Section 7).

Figure 9 (left panel) shows the temperature distribution in the central ($y = 0$) vertical plane and segments of magnetic fieldlines. The magnetic field vector is visualized by the arrows, which show the cross section of a flux tube that rises into the corona. Below the tube, there is a vertical current sheet, visualized by the (yellow) isosurface. The hot plasma, above and below the current sheet, is emitted by the reconnection jets, which blast from the upper and lower parts of the sheet with enhanced current density. The upward outflow contributes to the acceleration of the rising flux tube. The reconnection flow that is moving downwards, increases the temperature of arcade like structures, which are formed below the current sheet.

The right panel in Figure 9 contains a full view of the vertical current sheet below the rising flux tube and the topology of the fieldlines, which have been shown in the left panel. The blue fieldlines have been traced from the center of the cross section of the flux tube. They have been fully reconnected and they do not possess dips at the low atmosphere. They reach coronal heights and they generally represent the *central* part of the rising flux tube. The orange fieldlines have been traced from the hot arcade structure below the sheet. These are reconnected fieldlines that surround the main axis of the initial, emerging flux tube. Below the current sheet, the field adopts the form of hot loops with a strongly azimuthal nature with respect to the polarity inversion line of the emerging field.

Higher in the atmosphere, the formation of current layers is mostly linked with the rise of the newly formed flux tubes and the movement of high velocity outflows due to reconnection. The rise of the flux tubes inside the emerging system is not unhindered. The first fieldlines of the

emerging system that rise into the corona, create an ambient field for the flux tubes that are formed later on, due to internal reconnection. As the outer fieldlines of the tubes rise and expand, they approach the pre-existing field. Then, current layers may form at the interfaces between the upcoming set of fieldlines and the ambient fieldlines. The orientation of the fieldlines across these current layers resemble rotational discontinuites.

Due to the reconnection that occurs at the current sheets below the flux ropes, hot plasma outflow is expelled from the current sheets and is moving upward with high speed. These outflows are similar to the reconnection jets found in the simulations by Archontis & Hood (2008). The reconnection outflows are emitted vertically but when they reach a short distance beneath the center of the ropes they change direction and start to move sideways. The sideway motion of the plasma flow is due to the decrease of the gas pressure away from the center of the tube. Then the high-speed flows run across the fieldlines at the lower part of the magnetized envelope of the rising tubes. This induces a shearing of the fieldlines at lower heights compared to that of the fieldlines closer to the central region of the tube. As a result, thin current layers form between the fieldlines, which suffer from the shearing, and the fieldlines which have not been affected by the high-speed reconnection outflows.

It is worthwhile mentioning that it is likely that the current layers form along quasi-seperatrix layers (QSLs). In 3D magnetic field configurations, QSLs are narrow layers where there is a drastic change in the connectivity of the fieldlines. The concept of current sheet formation and reconnection in QSLs has been studied extensively in the past few years. Most of the experiments have used as an initial condition smooth magnetic configurations formed by a number of discrete flux concentrations. The discrete sources were moved by applied boundary motions and the formation of QSLs was studied by Priest & Demoulin (1995), Aulanier et al. (2005), Aulanier et al. (2006) and Demoulin (2006). One factor used in the previous studies to localize the QSLs and define some of their properies is the squashing degree, Q (Titov et al. 2002; Aulanier et al. 2005 and references therein). In our expeeriment, a preliminary estimation of the squashing degree indicates that sites of strong current concentrations develop preferentially in regions where the squashing degree is large. We believe that they are formed inside the expanding magnetized volume of the emerging region because of the repeated process of internal reconnection. A detailed study of the formation of QSLs and their connection to the sites with strong current density in similar flux emergence experiments will be undertaken in a forthcoming paper.

7. HEATING OF THE SIGMOIDAL STRUCTURE

The existence of many current structures along the S-shape structure is significant. The current structures are regions where fieldlines may reconnect and convert magnetic energy to thermal energy, bulk kinetic energy and accelerated particles. The reconnection process would then be an efficient means of heating and, thus, creating the emission that is observed from soft X-Ray sigmoids.

To further illustrate the filamentary structure of the sigmoidal current and the heating that occurs along it, we produce synthetic images of $\mathbf{J^2}$, which is proportional to the Joule heating term and ρ^2, which may account for the observed intensity in X-Rays. Here, we should mention that this is a very rough aproximation since our energy equation is adiabatic and, thus, extra heating sources (such as heat conduction, radiative transfer, etc.) are not included in the experiments. Thus, according to our considerations we estimate:

$$A = \int J^2 \, dz \tag{12}$$

and

$$B = \int \rho^2 \, dz. \tag{13}$$

The calculation of the *heating term* A and the *intensity term* B are done with respect to height, from the lower photosphere ($z = 55$) until well inside corona ($z = 200$). In addition, the integration is carried out only in the regions where the temperature has large values between 0.6 and 2.5 million Kelvin.

Figure 10 shows the result of the calculation of the terms A and B at three different times: $t = 140$ (top panel), $t = 168$ (middle panel) and $t = 184$ (bottom panel). The top-left panel shows that heating occurs mainly along the two *elbows* and it is still very weak at the central part of the emerging field. It also shows that the overal current in the emerging region is not a single (S-shaped) content object but consists of few layers where the temperature is enhanced. As we described in the previous sections, at this phase of the evolution the current density is large along the *Js* and reconnection of fieldlines occurs primarily along these currents (panel C, Fig. 5). Thus, the general picture of the distribution of heating along height described in the top panel is consistent with those resuts. The top-right panel shows that the *intensity term* keeps a good correlation with the *heating term*. Sites with very dense plasma are also hot. The brighter parts are located along the two main *elbows* but there are also other dense filamentary strands along the S-shaped surface.

The middle-left panel shows that the heating is still pronounced at the *elbows*, which now spread out and approach each other at the central region of the evolving field. There is still a narrow area with very little heating due to the fact that reconnection of fieldlines is limited. On the other hand, an important result is that now there are more hot loops or strands, which are formed sideways from the main bodies of the *elbows*. Also, the scrolls at the ends of each *elbow* reveal a more intermittent structuring. The hot structures that appear in this figure, can be reasonably interpreted as the signature of reconnection process occuring at current layers. It is worthwhile to mention that, the 3D visualization of the current density in Figure 8 shows indeed that the current density consists of many individual structures where reconnection of fieldlines is likely to occur. Thus, there is a qualitative agreement between the integration of heating along height and the 3D volume rendering of the total current density. Also, the middle-right panel shows that additional dense material start to cover a wider spatial range along the sigmoidal structure. The general distribution of the *intensity term* shows that it keeps getting more pronounced at the high-temperature regions.

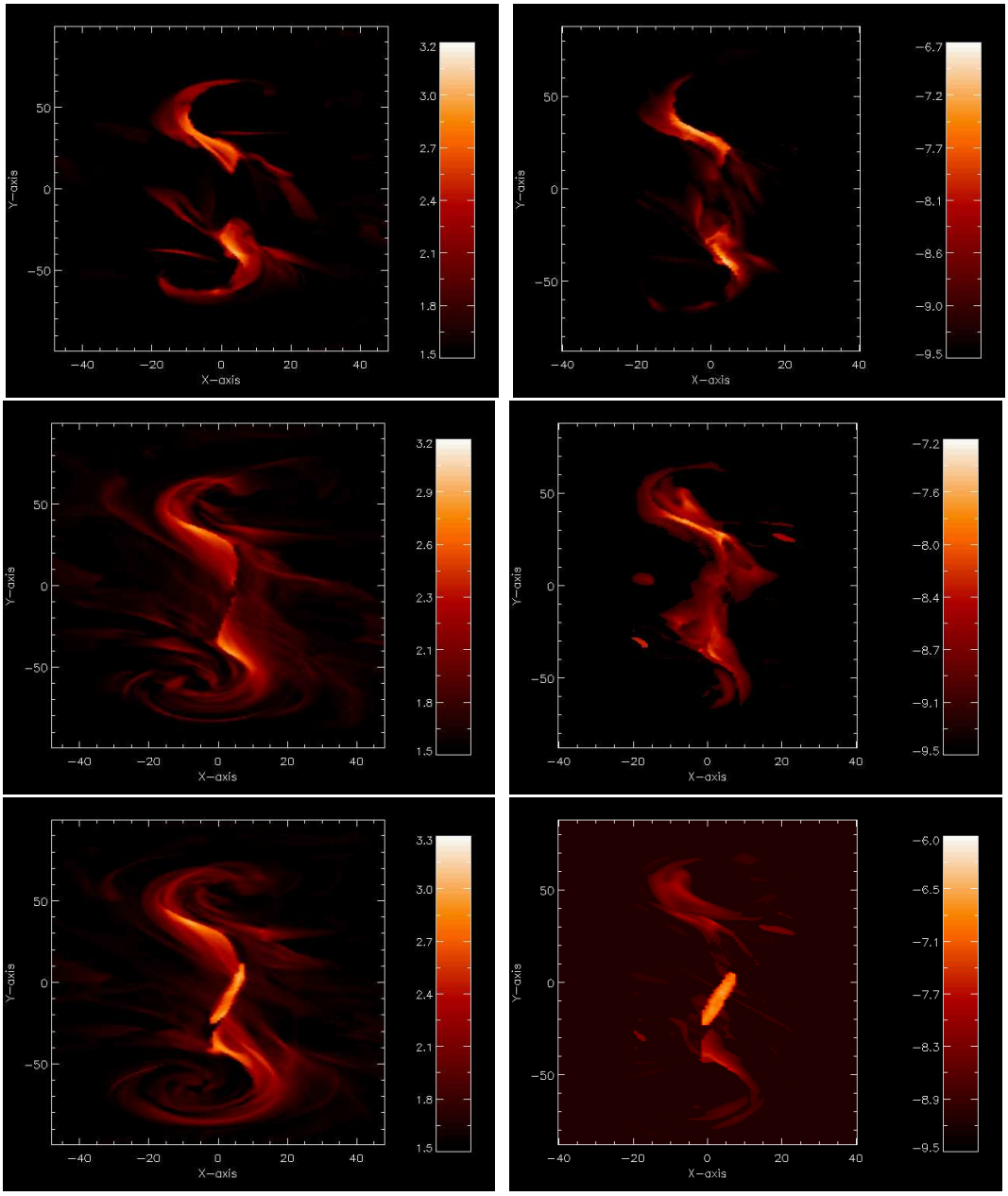

FIG. 10.— The evolution of the sigmoidal structure calculated by the integration of $\mathbf{J^2}$ (left column) and ρ^2 (right column) along height. Both terms are shown in a logarithmic scale. The times of the three snapshots are: $t = 140$ (top panel), $t = 168$ (middle panel) and $t = 184$ (bottom panel). A color version of this figure is available in the electronic edition of the Astrophysical Journal.

The bottom-left panel in Figure 10 shows a remarkable brightening at the central region of the sigmoidal structure. This is due to vigorous reconnection of fieldlines passing through a narrow volume between the *elbows*. Notice, that this is the same area where the heating was limited at $t = 168$ (middle panel). The difference with the earlier evolution is that now a current sheet is formed there and the apparent brightening corresponds to fieldlines succesively heated by internal reconnection. Before the flaring of the sigmoid, a flux tube is formed and rises from this central area to the outer atmosphere (see also Figure 8). The formation of this *central* flux tube occurs via reconnection, in a similar manner to the earlier formation of flux tubes above the *elbows*. The fieldlines that reconnect belong to opposite J-like bundles. The reconnection occurs mainly at their straight ends close to the central region of the emerging field. The result of this process is the formation of long, reconnected fieldlines that connect the two polarities of the emerging system and they have fully escaped into the corona.

A new, sharp, vertical current segment with a sheet-like shape is formed below the flux tube and the enhancment of temperature at the current structure manifests itself as a brightening, which appears shortly after the beginning of the rising motion of the flux tube. At low heights, the reconnected fieldlines below the rising flux

tube form an arcade of short and hot loops at the center of the sigmoidal structure. These hot structures may account for the short 'post-flare' like loops seen in some sigmoids. Similar, cusped-like, loops have been found in the simulations by Archontis & Hood (2008). The right panel in the last row of Figure 10 shows that the two *elbows* still contain relatively dense material. However, the most dense plasma is found at the central region of the sigmoidal structure and coincides with the intense heating occuring at the same area.

8. OBSERVATIONS OF SIGMOIDS

The results of our numerical experiments reveal that the dynamical emergence of a twisted flux tube leads to formation of a sigmoid with an intricate structure. Initially the sigmoid comprises two seperate *J-like* patterns but as the system evolves the internal structure of the sigmoid becomes more complex. It consists of many strong current layers (which persumambly are quasi-seperatrix layers) where intensive heating is taking place.

In February 2007, the X-ray Telescope (XRT) on board the Hinode satellite obtained high cadence data on the formation, evolution and eruption of a prominent coronal sigmoid. These were one of the first observations of such a feature on the Sun with high spatial and temporal resolution, which allowed the detailed analysis of the observations. Among other things, these observations revealed (as also described in our numerical experiments) that the overall S-shape of the sigmoid is due to many individual loops and is not defined by one, single X-Ray loop (McKenzie & Canfield 2008).

Figure 11 shows a comparison between XRT observations and the results from the numerical experiments at three different times: one at a phase where the two *elbows* are visible, one before the eruption and one after the eruption. The left and middle columns show isosurfaces of constant current density (the same as in Figure 8) and visualization of the *heating term* respectively (see also left panel in Figure 10). The right column consists of a series of XRT images of the sigmoid between 06:01UT and 08:59UT on 12 February. A qualitative comparison between the observations and the simulations reveal remarkable similarities in the geomerty and evolution of the sigmoidal structure. Firstly (top row), the S-shaped structure is more confined into the two *elbows*, which are dense and hot. During the evolution of the system (middle row), the XRT observations show that the overall structure appears to consist of more hot loops. In the simulations, it is likely that these loops are reconnected fieldlines in and around the newly formed current layers. Later on (bottom row), XRT observed a brightening at the middle part of the sigmoidal structure. McKenzie & Canfield (2008) speculated that this brightening is the sign of a cusped arcade that appeared after the eruption of a long flux rope from the central part of the S structure. In our simulations, a considerable temperature and density enhancment was also found around the central region, between the two *J-like* bundle of fieldlines. This is shown in the middle panel of the last row in Figure 11 and also in Figure 10. Moreover, the brightening in the middle appeared after the eruption of a flux rope from the same area. Underneath the rising flux tube, fieldlines form an arcade-like structure where the temperature is much higher than in the surrounding plasma. The rising flux tube and the hot and dense structure underneath, are shown in Figure 9.

9. DISCUSSION

This paper presents the results of a simulation of an emerging flux tube and the formation and evolution of a sigmoid, formed self-consistently by the emergence process. The sigmoid can be identified by either isosurfaces of current density, projected field lines or contours of integrated plasma density and current density squared. The general properties of the sigmoid formed are compared with observations of a sigmoid obtained with the Hinode X-Ray Telescope.

The numerical experiment begins with a single buoyant, Ω-shaped flux tube located at sub-photospheric layers. It is worthwhile to mention that the subsequent evolution is all self-consistent and no additional photospheric shearing motions are imposed. In keeping with other flux emergence simulations, the buoyant section of the tube initially rises towards the photosphere. However, once it reaches the stably stratified photosphere, the rise is halted and the field spreads out until the Parker (magnetic buoyancy) instability can be triggered. The subsequent evolution depends on the wavelength of the most unstable Parker mode. In our simulation, the length of the rising sub-photospheric field is approximately twice the length for the Parker mode and so there are potentially possible two regions of strong emergence at the photosphere. Shortly afterwards, the flux tube emerges through the photosphere and two *J-like* structure are seen. Subsequently, the *J-like* structures coalesce and form a more coherent *S-shaped* sigmoid. As the emergence process continues and flux tubes form through internal reconnection, the current structures become increasingly more fragmented. The sigmoid consists of many thin current sheets/layers where reconnection of fieldlines is vigorous and *continous*. The current sheets are formed at many different heights, from photosphere up into coronal heights. The loops which form the overall sigmoid are reconnected fieldlines heated by reconnection along the current layers.

Our simulation passed through many phases during the evolution of the magnetic field. One such phase has many features of the model by Titov & Demoulin (1999), which presents an equilibrium model of a sigmoid (consisted of two *J-like* bundles) and discusses the importance of bald-patches and bald-patch separatrix surfaces. Our simulation proceeds further with the formation of flux tubes through internal reconnection and the fragmentation of the current sheets/layers.

A key feature of the simulations is how the current structures evolve from simple distributed currents to highly fragmented, twisted sheets and layers. The observations also indicate an increase in the complexity of the soft X-ray emission as the sigmoid evolves. This may well be a universal plasma process. For example, Browning et al. (2008) showed how a single helical current sheet, formed by an ideal kink instability, fragmented during the Taylor relaxation of a coronal loop. Indeed, the relaxation process, whereby the plasma relaxes to a constant α force-free field with the same helicity as the initial configuration, can only occur if the plasma is sufficiently lubricated by the formation of many small-scale current sheets/layers. New experiments of this fragmen-

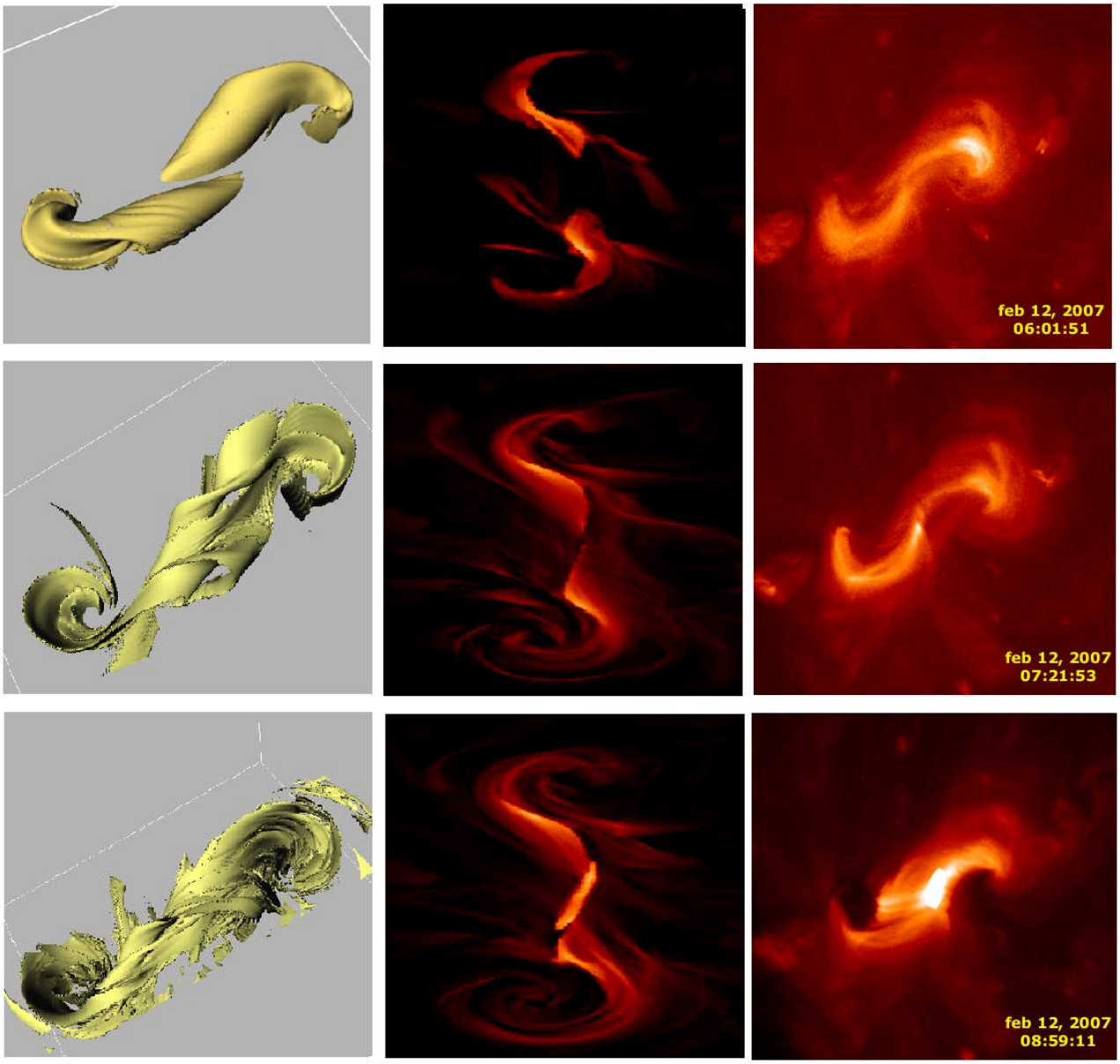

FIG. 11.— Comparison between the simulations (left and middle columns) and the XRT observations (right column). The left column shows the evolution of the constant current surfaces, the middle one shows corresponding snapshots of the *heating term* (see eq. 9) and the right column shows XRT images at three different times during the evolution of the sigmoidal structure. A color version of this figure is available in the electronic edition of the Astrophysical Journal.

tation/relaxation process need to be undertaken.

The simple comparison with observations was achieved by looking at synthetic images created by integrating the square of the current and plasma density over height and over a defined temperature range. This was only an initial attempt but it does provide encouraging similarities. Future work will include a more realistic energy equation, with thermal conduction and optically thin radiation, and will allow synthetic emissions that use the relevant instrument response function to be produced and compared directly with observations.

During the initial phase of the evolution of the system, the timescale of the simulation is proportional to $\beta^{\frac{1}{2}}$ and this puts an upper limit to the value we can choose to keep the running time of the simulation within reasonable bounds. Thus, given the parameters of our numerical experiment the timescale of the evolution of the sigmoid (from the formation until the eruption of the flux rope) is about 60 minutes. A modification of the parameters of the system (field strength, twist, initial height of the tube in the solar interior, size of the numerical domain, etc) could lead to formation of a sigmoidal structure that can persist for many hours. Obviously the time-scale of these sigmoids is different to the life-time of the long-lived coronal sigmoid presented in this paper. On the other hand, it is worthwhile to mention that Pevtsov (2002a) studied about 200 sigmoids, which were observed by Yohkoh, and found that about half of them persist

for less than one day. In any case, we expect that the general mechanism that is responsible for the evolution of complexity in sigmoidal structures, as has been described in previous sections of this paper, is applicable for both the short-lived and long-lived sigmoids.

An interesting issue is whether flux emergence is necessary for the build-up of complexity in sigmoids. In our simulations, flux emergence provides a means to follow the formation and evolution of sigmoids in a self-consistent manner. It also provides: the distribution of the line-of-sight magnetic field, B_z, at the photosphere, shearing photospheric motions and brings helicity into the system. Thus, it is not unlikely that mechanisms that provide these key ingredients will produce sigmoid structures in a similar manner to our flux emergence model.

From the observations, of the complex sigmoid presented in this paper, is still not clear whether at the very early stage of the evolution there is one 'active region' or two small seperate 'active regions ' which eventually interact and lead to the formation of the persistent sigmoid. One then might try to model the formation and evolution of such intricate sigmoids by studying the interaction of two bipolar regions. Archontis & Hood (2008) performed a 3D MHD experiment to study the interaction of two emerging flux systems, that rise through a highly stratified atmosphere. Not suprisingly, the initial results of that experiment showed a complex structure for the distributed sigmoidal current between the magnetic flux systems.

Further experiments are required for a direct comparison with observations and quantitative determination of our results. Also, for the cases where the observed sigmoids are associated with flux emergence comparison between the observed and simulated properties may allow us to determine the details of the pre-emergence subphotospheric flux system, which is a very important issue in flux emergence simulations. Obviously, this will require more observations that record the formation and evolution of sigmoids.

REFERENCES

Acheson, D. J., 1979, Solar Physics, 62, 63
Arber, T. D., Longbottom, A. W., Gerrard, C. L., & Milne, A. M., 2001, JCP, 171, 151
Archontis, V., 2008a, JGR, 113, A3
Archontis, V., Moreno-Insertis, F., Galsgaard, K., Hood, A.W, & O'Shea, E. 2004, A&A, 426, 1047
Archontis, V. & Hood, A. W., 2008, ApJ, 674, 2
Aulanier, G., Demoulin, P. & Grappin, R, 2005, A&A, 430, 1067
Aulanier, G., Pariat, E., Demoulin, P. & Devore, C. R., 2006, SoPh, 238, 2
Browning, P.K., Gerrard, C., Hood, A.W., Kevis, R. & van der Linden, R.A.M., 2008, A&A, 485, 837-848
Canfield, R.C., Hudson, H.S. & McKenzie, D.E., 1999, GeoRL, 26, 6, 627-630
Canfield, R.C., Kazachenko, M.D., Acton, L.W., Mackay, D.H., Son, J. & Freeman, T.L., 2007, ApJ, 671, 1, L81-L84.
Deluca, E.E., 2007, ASPC, 369, 19D
Demoulin, P., 2006, Advances in Space Research, 37, 7
Fan, Y., 2001, ApJ, 554, 1, L111-L114.
Fan, Y. & Gibson, S., 2003, ApJ, 589, 2, L105-L108.
Gerrard, C.L., Hood, A.W. & Brown, D.S., 2004, A&A, 222, 1, 79-94
Gibson, S. & Fan, Y., 2006, ApJ, 637, L65
Gibson, S.E., Fan, Y., Trk, T. & Kliem, B., 2006a, SSR, 124, 131-144
Golub, L., Deluca, E., Austin, G., Bookbinder, J., Caldwell, D. and 19 coauthors, 2007, SoPh, 243, 1, 63-86
Green, L.M., Kliem, B., Török, T., van Driel-Gesztelyi, L. & Attrill, G.D.R., 2007, SoPh, 246, 2, 365-391
Kusano, K., 2005, ApJ, 631, 2, 1260-1269
Magara, T. & Longcope, D.W., 2001, ApJ, 559, 1, L55-L59
Manchester, W.IV., Gombosi, T., DeZeeuw, D. and Fan, Y., 2004, ApJ, 610, 588-596
McKenzie, D.E & Canfield, R.C, 2008, ApJ, 481, 1
Moore, R.L, & LaBonte, B.J, 1980, In: *Solar and Interplanetary Dynamics*, IAU Symp.91, 207
Moore, R.L, & Roumeliotis, G., 1992, In: *Eruptive Solar Flares*, Springer, 69
Moore, R.L., Sterling, A.C., Hudson, H.S. & Lemen, J.R., 2001, ApJ, 552, 2, 833-848.
Pevtsov, A.A., Canfield, R.C. and Zirin, H., 1996, ApJ, 473, 533
Pevtsov, A.A., Canfield, R.C. and McClymont, A.N, 1997, ApJ, 481, 973
Pevtsov, A.A., 2002, SoPh, 207, 1, 111-123
Pevtsov, A.A., 2002a, COSPAR Colloquia Series, Volume 13, 125-134
Priest, E.R, Hood, A.W & Anzer, U., 1989, ApJ, 344, 1010
Priest, E.R & Demoulin, P., 1995, JGR, 100, A12
Rust, D.M. & Kumar, A., 1996, ApJ, 464, 199
Titov, V.S. & Demoulin, P., 1999, A&A, 351, 707
Titov, V.S., Priest, E.R & Demoulin, P., 1993, A&A, 276, 564
Trk, T. & Kliem, B., 2003, A&A, 406, 1043-1059
Trk, T., Kliem, B. & Titov, S. 2004, A&A, 413, L27-L30
Titov, V.S, Hornig, G. & Demoulin, P. 2002, JGR, 107, A8
van Ballegooijen, A. A. & Mackay, D. H., 2007, ApJ, 659, 1713